Reduction of vortex-induced vibrations of a cantilevered hydrofoil with passive piezoelectric shunt

Arthur Haudeville, Xavier Amandolese, Boris Lossouarn, Christophe Giraud-Audine, Olivier Thomas

25·29 August 2024
inter.noise
NANTES FRANCE

Reduction of vortex-induced vibrations of a cantilevered hydrofoil with passive piezoelectric shunt

Arthur Haudeville [1], Xavier Amandolese [2] and Boris Lossouarn [3]
Conservatoire national des arts et métiers (Cnam), LMSSC
292 Rue Saint-Martin, 75003, Paris, France

Christophe Giraud-Audine [4] and Olivier Thomas [5]
Arts et Metiers Institute of Technology (Ensam), L2EP, LISPEN
8 bd. Louis XIV, 59046 Lille, France

ABSTRACT

This work first investigates the ability of a low order fluid-structure model to fit the vortex-induced vibrations (VIV) observed on a truncated hydrofoil in a hydrodynamic tunnel. A particular VIV area is scrutinized, for which a hydrodynamic excitation mechanism due to a Kármán-type vortex wake organization successively locks the first torsional and second bending mode of the cantilevered hydrofoil. Coupling two structure oscillators with a Van der Pol wake oscillator satisfactorily reproduces the amplitude response and the lock-in frequency. In order to build a low order model allowing to optimize control strategy, a fourth degree of freedom corresponding to the electric circuit of a resonant piezoelectric shunt has been added. Composed of an inductance and a resistance connected to a piezoelectric patch, the passive shunt was tuned to minimize the vibration amplitude in the frequency lock-in range. Model predictions are finally compared with experimental results.

1. INTRODUCTION

Flow-induced vibrations (FIV) of hydrodynamic lifting structures have to be considered to avoid destructive or fatigue behaviors and improve performances. According to Blake [1], vibrations of hydrofoil operating at low angles of attack can be due to either a random excitation mechanism (generated by the turbulence of the incoming flow or the turbulent boundary layer on the hydrofoil surface) or a harmonic flow excitation generated by a periodic vortex shedding from the trailing edge. In the latter case, referred as vortex-induced vibration (VIV), tonal noise emission can also be observed. Both the hydrofoils with either a blunt trailing-edge or a sharp trailing edge are concerned by VIV and tonal noise emissions. For the former, it is the consequence of a Kármán-type vortex wake organization [2]. For the latter, it can be due to a hydroelastic coupling between a boundary layer transition mechanism occurring close to the trailing edge and a structural mode of

[1] arthur.haudeville@ensam.eu

[2] xavier.amandolese@lecnam.net

[3] boris.lossouarn@lecnam.net

[4] christophe.giraud-audine@ensam.eu

[5] olivier.thomas@ensam.eu

the hydrofoil involving significant displacement in the trailing edge area [3]. For both scenarios, vibrations of significant amplitude can be observed in a limited range of velocity which make this fluid-structure behavior be classified as vortex-induced vibrations (VIV). Regarding structures of circular or low aspect ratio cross section, of great importance for wind and off-shore engineering, numerous phenomenological models have been developed in the past decades [4]. Recently, a low order model derived from the Facchinetti, de Langre and Biolley wake oscillator model [5], has also been proposed by Amandolese et al. [6], to fit the bending or torsional VIV observed on a cantilevered rectangular flat plate in a hydrodynamic tunnel. This paper focuses on a truncated NACA 66-306 hydrofoil at low angle of attack studied by Watine [7] through experiments conducted in the hydrodynamic tunnel of the French Naval Academy Research Institute (IRENav). A short range of Reynolds number $2.55\times105 \leq Re \leq 4.68\times105$ (i.e. mean flow velocity range : $3 \leq U \leq 5.5$ [m.s^{-1}]), for which a Kármán-type vortex wake organization successively locks the first torsional and second bending mode of the cantilevered hydrofoil, is scrutinized. Following the work of Amandolese et al. [6], an adapted and enhanced low order hydroelastic model is developed in section 2 and the set of associated parameters that best fit the experimental results in both amplitude response and frequency lock-in are identified in section 3. An electro-mechanical equation of a piezoelectric patch placed on the hydrofoil is then coupled to the previous model in section 4. Following the work of Watine [7], a single piezoelectric patch is considered for the mitigation of both torsional and bending vibrations. Model predictions are finally compared with experimental results, prior to a conclusion.

2. VIV MODEL

The cantilevered hydrofoil has a constant section (represented in Fig. 1) along a span $s = 191$ mm. It is a NACA 66-306 section for which the trailing edge is truncated at 85% of the original chord, so its new chord length is $B = 85$ mm. The maximum thickness, located at 45.46% of the original chord, is chosen as the characteristic length $D = 6.13$ mm that includes the extra thickness of 0.13 mm due to the surface treatment applied to reduce corrosion.. Then, the truncated hydrofoil has a chord to thickness ratio $B/D = 13.9$ and a zero angle of attack (maximal uncertainty of 0.1 deg). For more details about the hydrofoil tested at the IRENav hydrodynamic tunnel, see [7].

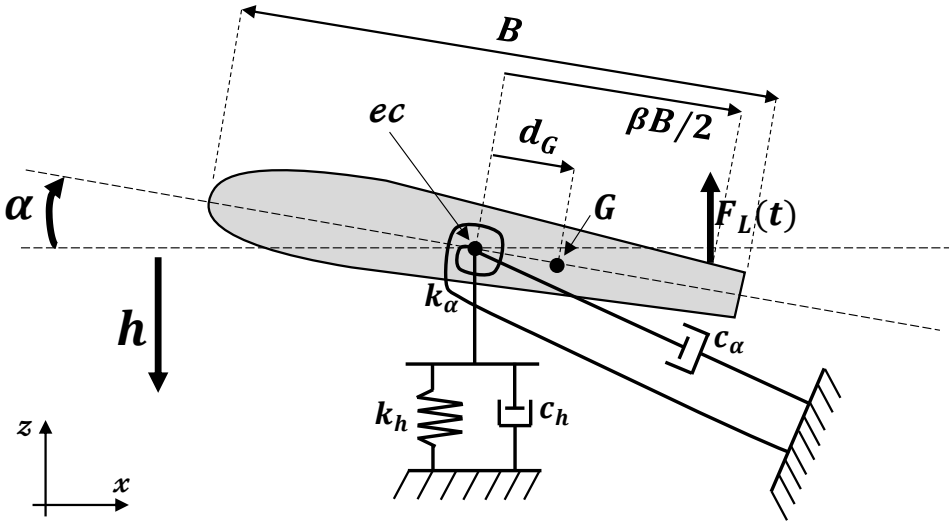

Figure 1: Equivalent model, of the generalized constant section along the span, of the truncated hydrofoil.

As reported in Fig. 1, we assume that the elastic center is located at the mid-chord and that the center of mass G may not coincide with the elastic center, introducing a parameter ($d_G \neq 0$) that is the distance from the elastic centre to the centre of gravity (positive toward the trailing edge).

Hydrodynamic excitation mechanism is due to a Kármán-type vortex wake organization that produces an unsteady lift for which the centrer of pressure is unknown. As proposed in [6], an unknown distance β, in semi-chord, is introduced (see Fig. 1). Angular and vertical displacements of the hydrofoil (α positive nose up and z positive up) are considered and represented with Kelvin-Voigt models for torsional and bending deformations respectively.

2.1. Structural oscillators

The Rayleigh's method is used to decompose in space and time the bending and torsion deformation of the cantilevered hydrofoil, $z(y,t) = \Phi_z(y)\, q_z(t)$ and $\alpha(y,t) = \Phi_\alpha(y)\, q_\alpha(t)$ respectively. Where Φ_z [−] is the second mode shape in bending and Φ_α [−] is the first mode shape in torsion of a cantilevered flat plate [8], q_z [m] and q_α [−] the corresponding generalized coordinates.Assuming that the center of mass G does not coincide with the elastic center ($d_G \neq 0$), the kinetic energy of the system can be written

$$\mathcal{T} = \frac{1}{2}\left[\int_0^s I_{tot}\Phi_\alpha^2\, dy\right]\dot{q_\alpha}^2 - \left[\int_0^s s_\alpha \Phi_\alpha \Phi_z\, dy\right]\dot{q_\alpha}\dot{q_z} + \frac{1}{2}\left[\int_0^s M_{tot}\Phi_z^2\, dy\right]\dot{q_z}^2 \tag{1}$$

$$= \frac{1}{2}I_\alpha^*\dot{q_\alpha}^2 - S_\alpha^*\dot{q_\alpha}\dot{q_z} + \frac{1}{2}M_z^*\dot{q_z}^2, \tag{2}$$

where I_α^* $\left[\text{kg.m}^2\right]$ is the generalized moment of inertia about the elastic center, M_z^* [kg] is the generalized mass and S_α^* [kg.m] is the generalized static momentum. $M_{tot} = m_z + m_{zu}$ $\left[\text{kg.m}^{-1}\right]$ and $I_{tot} = I_\alpha + I_{\alpha u}$ [kg.m] are the total lineic mass and moment of inertia (including the added fluid) and $S_\alpha = M_{tot}\, d_G$ [kg] is the lineic static momentum. The lineic mass $m_z \approx 1.1309$ kg.m^{-1} and moment of inertia $I_\alpha \approx 5.10^{-4}$ kg.m have been computed using the airfoil section geometry and the material (aluminium) density $\rho_s = 2650$ kg.m^{-3}. Air to water frequency ratios permit to determine fluid-added mass $m_{zu} = m_z\left[\left(f_{z,air}/f_z\right)^2 - 1\right] \approx 3.8771$ kg.m^{-1} and inertia $I_{\alpha u} = I_\alpha\left[\left(f_{\alpha,air}/f_\alpha\right)^2 - 1\right] \approx 12.10^{-4}$ kg.m where $f_{z,air}$, $f_{\alpha,air}$ and f_z, f_α are the natural frequencies of the first torsion and second bending modes measured in air and water by Watine [7].

The potential and dissipation energy of the system can be written [8] as

$$\mathcal{U} = \frac{1}{2}K_\alpha^* q_\alpha^2 + \frac{1}{2}K_z^* q_z^2 \quad \text{and} \quad \mathcal{D} = \frac{1}{2}C_\alpha^*\dot{q_\alpha}^2 + \frac{1}{2}C_z^*\dot{q_z}^2, \tag{3}$$

where $K_\alpha^* = I_\alpha^*\omega_\alpha^2$ and $K_z^* = M_z^*\omega_z^2$ are respectively the generalized stiffness in torsion and in bending of the hydrofoil, which are derived from the Rayleigh's quotients of a natural mode. Where $\omega_\alpha = 2\pi f_\alpha$ and $\omega_z = 2\pi f_z$ are the natural angular frequencies of the first torsion mode and second bending mode respectively. We also define $C_\alpha^* = 2\zeta_\alpha^{tot}\omega_\alpha I_\alpha^*$ and $C_z^* = 2\zeta_z^{tot}\omega_z M_z^*$ the generalized Rayleigh's dissipation functions in torsion and bending respectively. With the total damping ratios $\zeta_\alpha^{tot} = \zeta_\alpha + \zeta_{\alpha u}$ and $\zeta_z^{tot} = \zeta_z + \zeta_{zu}$, defined as the sum of the modal damping ratio of the hydrofoil measured in water with zero flow velocity ($\zeta_\alpha = 0.317$ % and $\zeta_z = 0.669$ %) and velocity dependent fluid added damping ratios $\zeta_{\alpha u}$ and ζ_{zu} derives from Theodorsen's analytic solution [6, 9]:

$$\zeta_{\alpha u} = p_{\alpha u}\frac{\rho U B^3}{4\omega_\alpha I_{tot}}\left[\frac{\pi}{8} - \left(\frac{dC_L}{d\alpha}\right)_{\alpha_0} C_\alpha\right] \quad \text{and} \quad \zeta_{zu} = p_{zu}\frac{\rho U B}{4\omega_z M_{tot}}\left(\frac{dC_L}{d\alpha}\right)_{\alpha_0} C_z. \tag{4}$$

With ρ the density of the water, $(dC_L/d\alpha)_{\alpha_0} \approx 2\pi$ the slope of the lift coefficient around the wedge angle, U the mean flow velocity, $p_{\alpha u} = 0.25$ and $p_{zu} = 0.15$ weight coefficients suggested in [6] and, in the considered range of reduced frequency $\kappa = \frac{B\omega}{U}$: $C_\alpha = \frac{F(\kappa)}{16} + \frac{G(\kappa)}{4\kappa} \approx 0.0312$ and $C_z = F(\kappa) \approx 0.5$. This approximation of the damping ratios avoid the use of the real $F(\kappa)$ and the imaginary $G(\kappa)$ parts of the Theodorsen's function (themselves composed of Bessel's functions dependent on the flow velocity). Instead, these approximated damping ratios are simply linearly dependent with respect to the flow velocity.

2.2. Hydrodynamic load and structural coupling

The generalized momentum $Q_\alpha(y,t)$ and the generalized lift force $Q_z(y,t)$ are projected on the first torsion and second bending deflection shape respectively. Loading terms derived form structural equations of motion can, then, be expressed with the lineic lift force $F_L(t)$ and momentum $M_{ec}(t)$ as

$$\frac{Q_\alpha}{I^*_\alpha} = \frac{M_{ec}(t)}{I_{tot}} \frac{\int_0^s \Phi_\alpha(y)\,dy}{\int_0^s \Phi_\alpha(y)^2\,dy} = \frac{M_{ec}(t)}{I_{tot}} S_{\Phi\alpha} \quad \text{and} \quad \frac{Q_z}{M^*_z} = \frac{F_L(t)}{M_{tot}} \frac{\int_0^s \Phi_z(y)\,dy}{\int_0^s \Phi_z(y)^2\,dy} = \frac{F_L(t)}{M_{tot}} S_{\Phi z}. \tag{5}$$

Shape functions $\Phi_\alpha(y)$ and $\Phi_z(y)$ are chosen as the first torsion and second bending modes shapes of a cantilevered flat plate [8]. With a normalization of both deflection shapes such as $\Phi_\alpha(s) = \Phi_z(s) = 1$, modes shapes coefficients are evaluated to $S_{\Phi\alpha} = 4/\pi$ and $S_{\Phi z} \approx 0.8679$. With a similar approach, we can also express accelerating coupling coefficients between structural oscillators which derive from coupling effects between the two modes:

$$\frac{S^*_\alpha}{I^*_\alpha} = \frac{M_{tot}}{I_{tot}} \frac{\int_0^s \Phi_\alpha(y)\,\Phi_z(y)\,dy}{\int_0^s \Phi^2_\alpha(y)\,dy}\,d_G = \frac{M_{tot}}{I_{tot}}\,S_{\Phi\alpha g}\,d_G \quad \text{and} \quad \frac{S^*_\alpha}{M^*_z} = \frac{\int_0^s \Phi_\alpha(y)\,\Phi_z(y)\,dy}{\int_0^s \Phi^2_z(y)\,dy}\,d_G = S_{\Phi z g}\,d_G, \tag{6}$$

where $S_{\Phi\alpha g} \approx -0.1937$ and $S_{\Phi z g} \approx -0.3876$.

About the loading applied on the hydrofoil, based on previous works on such structure with axial flow [4, 10–12], the unsteady lineic lift force gives $F_L(t) = \frac{1}{2}\rho\,B\,U^2\,C_L(t)\,\left[\mathrm{N.m^{-1}}\right]$ where $C_L(t)$ is the unsteady lift coefficient. The lift force is considered close to the trailing edge but with an unknown center of pressure. Then, the lineic momentum about the elastic center is developed as $M_{ec}(t) = F_L(t)\,\frac{\beta B}{2}$ [N] and equations of motions can be written as

$$\begin{cases} \ddot{q}_\alpha + 2\zeta^{tot}_\alpha \omega_\alpha \dot{q}_\alpha + \omega^2_\alpha q_\alpha - \theta_\alpha \ddot{q}_z = -M_v\,C_L(t) \\ \ddot{q}_z + 2\zeta^{tot}_z \omega_z \dot{q}_z + \omega^2_z q_z - \theta_z \ddot{q}_\alpha = F_v\,C_L(t) \end{cases}, \tag{7}$$

where

$$M_v = A_{q\alpha}\,S_{\Phi\alpha}\,\beta, \quad F_v = A_{qz}\,S_{\Phi z} \tag{8}$$

$$A_{q\alpha} = \frac{\rho\,B^2\,U^2}{4I_{tot}}, \quad A_{qz} = \frac{\rho\,B\,U^2}{2M_{tot}}, \quad \theta_\alpha = \frac{M_{tot}}{I_{tot}} S_{\Phi\alpha g}\,d_G, \quad \text{and} \quad \theta_z = S_{\Phi z g}\,d_G. \tag{9}$$

2.3. Wake oscillator

As shown in [6], harmonic forced system model fails to predict amplitude response. On the contrary, strongly coupled model with a wake oscillator associated to the Strouhal number has given good fit to the shape of amplitude response. In this model, the Kármán vortex wake loading is modeled by a Van der Pol oscillator, as in Eq. (10), where is introduced a dimensionless variable q_v that can be interpreted as a reduced vortex lift coefficient $q_v = 2C_L(t)/C^0_L$, where C^0_L is the static lift coefficient. Because vibrations are considered small, we can write that $q_{\alpha z} = \frac{B}{2}\sin(-q_\alpha) \approx -\frac{B}{2}q_\alpha$ and the Kármán vortex wake loading becomes

$$\ddot{q}_v + \omega_v \varepsilon \left(q^2_v - 1\right)\dot{q}_v + \omega^2_v q_v = A_z \ddot{\bar{q}}_z + A_\alpha \ddot{\bar{q}}_{\alpha z}. \tag{10}$$

We introduce the growth rate coefficient ε, the angular frequency of the hydrodynamic excitation $\omega_v = 2\pi St\,U/D$ and St the Strouhal number. Acceleration coupling has been considered with two unknown coupling coefficients A_α and A_z. The coupled system (Eq. (7) and Eq. (10)) is proposed in a non-dimensional form by introducing the dimensionless time $\tau = \omega_v t$ and the reduced vibration amplitudes relatives to the chosen characteristic thickness of the hydrofoil:

$$\bar{q}_z = \frac{q_z}{D} \quad \text{and} \quad \bar{q}_{\alpha z} = \frac{q_{\alpha z}}{D}. \tag{11}$$

From non-dimensional form, we introduce the structure to fluid frequency ratio $\delta_i = \omega_i/\omega_v$, the reduced flow velocity $U_{r_i} = U/f_i D$ and the relation between them $St\, U_{r_i} = 1/\delta_i$ (valid for both the first torsion mode and the second bending mode, using $i = \{\alpha, z\}$). We also introduce the dimensionless mass number $\mu_z = M_{tot}/(\rho B^2)$ and the inertia number $\mu_\alpha = I_{tot}/(\rho B^4)$. Finally, the coupled system of Eq. (7) and Eq. (10) can be written

$$\begin{cases} \ddot{\bar{q}}_{\alpha z} + 2\zeta_\alpha^{tot}\delta_\alpha \dot{\bar{q}}_{\alpha z} + \delta_\alpha^2 \bar{q}_{\alpha z} + \bar{\theta}_\alpha \ddot{\bar{q}}_z = \bar{M}_v q_v \\ \ddot{\bar{q}}_z + 2\zeta_z^{tot}\delta_z \dot{\bar{q}}_z + \delta_z^2 \bar{q}_z + \bar{\theta}_z \ddot{\bar{q}}_{\alpha z} = \bar{F}_v q_v \\ \ddot{q}_v + \varepsilon\left(q_v^2 - 1\right)\dot{q}_v + q_v = A_z \ddot{\bar{q}}_z + A_\alpha \ddot{\bar{q}}_{\alpha z} \end{cases} \quad \text{with} \quad \begin{cases} \bar{M}_v = \bar{A}_{q\alpha}\, \beta\, C_L^0\, S_{\Phi\alpha} \\ \bar{F}_v = \bar{A}_{qz}\, C_L^0\, S_{\Phi z} \end{cases}, \tag{12}$$

where the dependent fluid-added damping ratios in Eq. (4), the fluid coupling factors and the structural accelerating coupling coefficients in Eq. (9) written using dimensionless numbers become

$$\bar{\zeta}_{\alpha u} = p_{\alpha u}\, \frac{U_{r\alpha}}{8\mu_\alpha \pi}\, \frac{D}{B}\left[\frac{\pi}{8} - \left(\frac{dC_L}{d\alpha}\right)_{\alpha_0} C_\alpha\right], \quad \bar{\zeta}_{zu} = p_{zu}\, \frac{U_{rz}}{8\mu_z \pi}\, \frac{D}{B}\left(\frac{dC_L}{d\alpha}\right)_{\alpha_0} C_z \tag{13}$$

$$\bar{A}_{q\alpha} = \frac{1}{64\pi^2 St^2 \mu_\alpha}\frac{D}{B}, \quad \bar{A}_{qz} = \frac{1}{16\pi^2 St^2 \mu_z}\frac{D}{B}, \quad \bar{\theta}_\alpha = \frac{B}{2}\,\theta_\alpha, \quad \text{and} \quad \bar{\theta}_z = \frac{2}{B}\,\theta_z. \tag{14}$$

3. NUMERICAL RESULTS FROM TIME-DOMAIN SIMULATION

According to the coupled system in Eq. (12), a set of six parameters C_L^0, β, d_G, ε, A_α and A_z have to be identified. It is done in this section by comparing numerical results to experiments using a trial-and-error process allowing to highlight the effects of each parameter on the amplitude and frequency response. Resolution of non-linear ordinary differential equation (ODE) as Eq. (12) can be done by numerical integration approach, such as the Runge-Kutta method (here, using the 4-order algorithm). Such method necessitates to formalize equations to the form $\dot{X} = f(X, t)$. After a transient regime, the periodic solution is extracted and RMS values are calculated for each mean flow velocity. Results are compared to RMS experimental data. Experimental data are compared to the total contribution of both torsion and bending motions in dimensionless RMS amplitudes of vibrations with respect to the fluid velocity. Which can be written as in Eq. (15) since deflection shape functions have been normalized:

$$\bar{w}_z = \Phi_z(s)\,\bar{q}_z + \Phi_\alpha(s)\,\bar{q}_{\alpha z} = \bar{q}_z + \bar{q}_{\alpha z} \quad [RMS]. \tag{15}$$

Following fitting of the parameters has also been completed with the help of experimental frequencies. Numerical frequencies are extracted from the power spectral density (PSD) of the periodic signal of the coupled system. Since generalized coordinated $\bar{q}_{\alpha z}$ and $\bar{q}_z$ have different amplitudes but identical frequencies, both can be used to calculate the PSD (here, $\bar{q}_{\alpha z}$). The PSD itself, $S_{xx}(f) = |\hat{x}_e|^2/(T_e\, n_e)$, is calculated from the Fourier transform of the chosen signal $\hat{x}_e$, normalized by the number of sample n_e constituting the signal and over the dimensionless period of the signal T_e. Plotted experimental frequencies are maximal values of the PSD regardless the various peaks existing. The aim is to best fit numerical frequencies to experimental ones at the frequency leap's location. This leap between the natural mode frequency of torsion and bending one occurs at $4.6 \leq U \leq 4.7\,\mathrm{m.s^{-1}}$.

3.1. Identification of the model parameters

Note that experimental determination of the Strouhal number in [7] reflects two fluids excitation which are characterized by two Strouhal numbers $St_2 = 0.34$ (due to a Kármán vortex shedding) and $St_1 = 0.49$ (most likely due to a shear layer instability), which seems to merge at lock-in with the first torsional mode. To simplify the VIV coupled model, only one fluid excitation has been considered here at an intermediate Strouhal number $St = 0.41$. Which is here sufficient for the purpose of

vibration analysis and control. One can also notice, that a relation may exist between the Strouhal number and the growth rate coefficient ε of the Van der Pol equation because of this last coefficient which modifies the fluid natural frequencies and so the Strouhal number. The Van der Pol equation used in Eq. (10) for modeling the fluid oscillator may not be the most appropriate if such evolution has to be considered. In an objective of estimation of vibration amplitudes, it is enough to fix the Strouhal number and adapt the growth rate coefficient to fit back lock-in frequencies. Therefore, for $St = 0.41$, numerical calculation in Fig. 2 shows that $\varepsilon = 0.75$ best fits experimental lock-in frequencies.

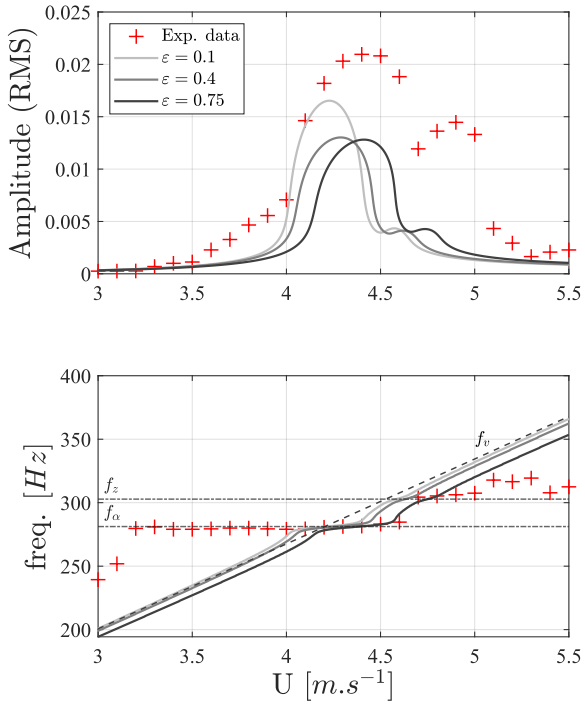

Figure 2: Coupled model versus experiment; $C_L^0 = 0.008$, $\beta = 1$, $d_G = 0$, $A_\alpha = 15$, $A_z = 15$ and three sets of parameter ε.

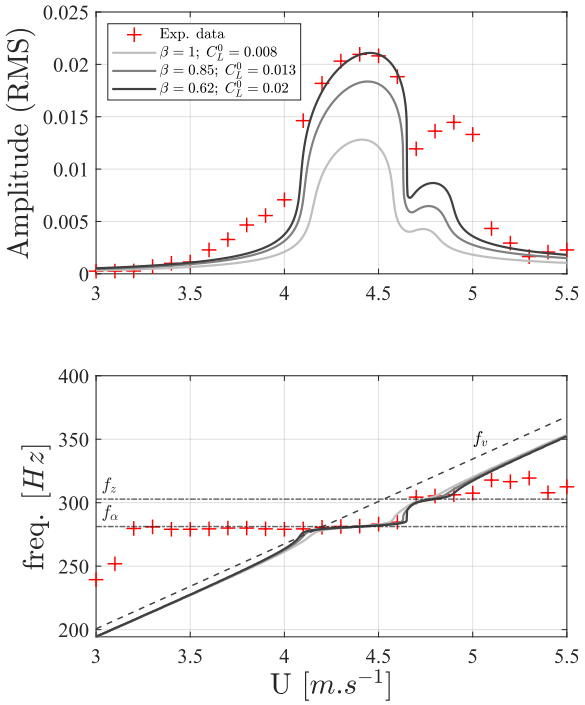

Figure 3: Coupled model versus experiment; $\varepsilon = 0.75$, $d_G = 0$, $A_\alpha = 15$, $A_z = 15$ and three sets of parameter β and C_L^0.

Based on the work of Amandolese et al. [6], static lift coefficient have been first set to the ones optimized for the Kármán vortex shedding on a flat plate : $C_L^0 = 0.008$. The pressure center position has been set at the trailing edge, i.e. $\beta = 1$. The distance between the elastic center and the center of gravity is initialized at $d_G = 0$. Accelerating coupling parameters have been taken lower than the one in [6], and initialized at $A_\alpha = A_z = 15$, since both contributes at once in our case. Amplitude of vibrations at the first torsion mode lock-in is fitted with the static lift coefficient C_L^0. Simultaneously, the β parameter is fitted such that the second bending mode related peak gains in amplitude relatively to the torsion mode peak. Best fitted parameters $C_L^0 = 0.02$ and $\beta = 0.62$, as shown in Fig. 3, allow to satisfactorily catch the amplitude and frequency response at lock-in with the first torsion mode while improving the lock-in with the second bending mode. With this value of β, the center of pressure of the lift force from the mid-chord is strongly displaced from the trailing edge. It could be coming from the simplification of the model at one fluid excitation and of fixed position of the elastic center at the mid-chord. Regarding the parameter d_G, it mostly affects vibrations of the bending mode and increases its lock-in range, as one can observe in Fig. 4. Better results in amplitudes of vibrations and lock-in range are obtained for $d_G = -3$ mm (the sign means that the center of gravity G is placed upstream of the elastic center, refer to Fig. 1). Finally, the accelerating coupling coefficients A_α and A_z of the Van der Pol equation mainly affect the lock-in ranges of their respective mode. As shows in Fig. 5, good fit of the coupling coefficients are obtained for $A_\alpha = 21$ and $A_z = 12$. With this last fitting, one can adjust the static lift coefficient to $C_L^0 = 0.0202$ in order to best fits maximal amplitudes of vibrations.

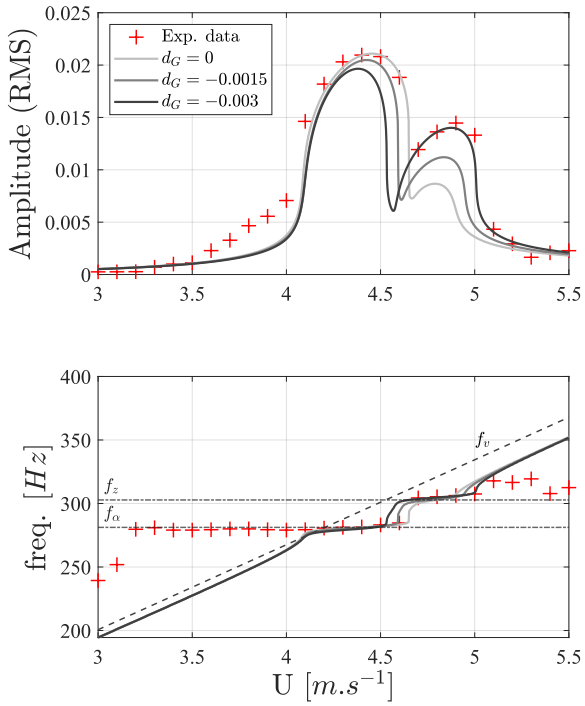

Figure 4: Coupled model versus experiment; $\varepsilon = 0.75$, $C_L^0 = 0.02$, $\beta = 0.62$, $A_\alpha = 15$, $A_z = 15$ and three sets of parameter d_G.

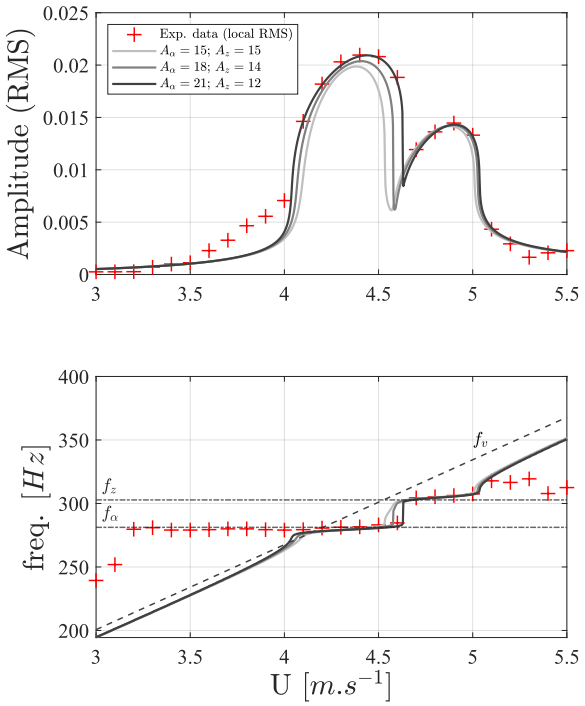

Figure 5: Coupled model versus experiment; $\varepsilon = 0.75$, $C_L^0 = 0.0202$, $\beta = 0.62$, $d_G = -0.003$ and three sets of parameters A_α and A_z.

3.2. Discussion

Best fitted parameters are summarized in Tab. 1. Adaptation of the VIV model from Amandolese et al. [6] gives good fits of amplitudes and frequencies compared to local RMS experimental data [7]. Note that prior to the lock-in of the hydrodynamic excitation (considered here at $St = 0.41$) and the first torsion mode, experiments results show an extended lock-in range starting from $U \approx 3.2\,\mathrm{m.s^{-1}}$. It can be due to a combination of turbulent-induced vibrations and to a hydrodynamic excitation associated to the strouhal number $St = 0.49$ observed experimentally. This hydrodynamic excitation mechanism is supposed to be the consequence of an impinging shear layer instability for which the pressure center, close to the mid-chord, slightly affect the amplitude response for $3.5 < U < 4\,\mathrm{m.s^{-1}}$ [6]. At last, regarding amplitude evolution, it seems that the solution has instabilities which could be predicted by continuation methods of calculation.

Table 1: Optimized parameters of the coupled VIV model for the first torsion mode and the second bending mode of the truncated hydrofoil.

Quantity	**Symbol**	**Value**
Amplitude lift coefficient	C_L^0	0.0202
Pressure center distance from the mid-chord	β	0.62
Growth rate coefficient	ε	0.75
Distance from the elastic center to gravity center	d_G	-0.003
Torsion acceleration coupling parameter	A_α	21
Bending acceleration coupling parameter	A_z	12

4. PASSIVE PIEZOELECTRIC SHUNT DAMPING

Vibration control using piezoelectric materials, with active and passive shunt, has already demonstrated good performance for structural damping [13, 14]. Using the piezoelectric effect, mechanical energy of a vibrating structure is converted to electrical energy (see Fig. 6) which may be dissipated through a resistance by Joule effect. Passive piezoelectric damping are traditionally resistive with simply a resistance (R-shunt) or resonant with a resistance and an inductance (RL-shunt) [15]. Greater vibration reduction are observed with resonant piezoelectric shunts since the shunt will also counteract the oscillations thanks to the occurrence of an electrical resonance [13]. Note that a piezoelectric patch is equivalent to a capacitor of capacitance C [$A^2.s^4.kg^{-1}.m^{-2}$]. Then, we define a voltage V [$kg.m^2.A^{-1}.s^{-3}$] and a current $\dot{Q}$ [A].

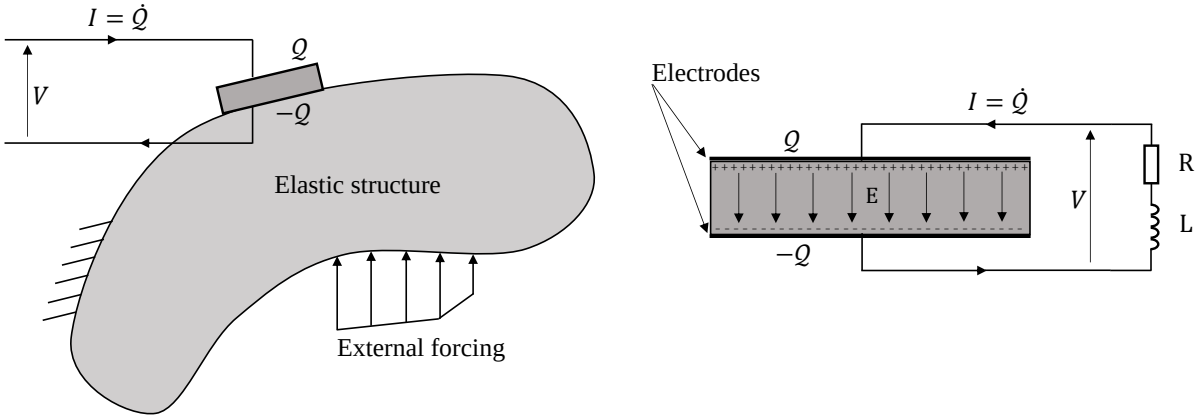

Figure 6: (left) An arbitrary elastic structure with a piezoelectric patch. (right) The piezoelectric patch subjected to a potential difference V, its electrodes containing the free electric charges Q and $-Q$ and the electrical circuit with a resistance R and an inductance L in series.

Following previous works [7, 16, 17], the resonant shunt is modeled in this section. Indeed, in the suction side of the hydrofoil studied in [7], a MFC piezoelectric patch of the type *M8557F1* had been integrated. Electrodes of the patch are connected, in series, with an inductance of value L [$kg.m^2.A^{-2}.s^{-2}$] and a resistance of value R [$kg.m^2.A^{-2}.s^{-3}$] (see Fig. 6). Then, the potential difference between electrodes can be rewritten using Kirchhoff's law with the inductance and the resistance of the circuit as

$$V = -L\ddot{Q} - R\dot{Q}. \tag{16}$$

Natural frequencies of a structure with piezoelectric patch are obtained with electrodes in short-circuit so that the electrical field is null and the piezoelectric effect does not occur. We keep ω_α and ω_z notation for the short-circuit angular frequencies of the first torsion mode and the second bending mode of the hydrofoil respectively, where the stiffness of the piezoelectric patch material is taken into account.

4.1. Shunted VIV model

Starting from the dimensional mechanical system in Eq. (7) with the angular generalized coordinate brought to its equivalent displacement, and adding a piezoelectric coupling between the hydrofoil and the electric circuit, one can express the electro-mechanical model as [13, 18]

$$\begin{cases} \ddot{q}_{\alpha z} + 2\zeta_\alpha^{tot}\omega_\alpha\dot{q}_{\alpha z} + \omega_\alpha^2 q_{\alpha z} + \bar{\theta}_\alpha\ddot{q}_z = M_v C_L(t) + \dfrac{\beta_\alpha^2}{I^*}\chi_\alpha V \\ \ddot{q}_z + 2\zeta_z^{tot}\omega_z\dot{q}_z + \omega_z^2 q_z + \bar{\theta}_z\ddot{q}_{\alpha z} = F_v C_L(t) + \dfrac{1}{M^*}\chi_z V \\ CV - Q + \chi_\alpha q_{\alpha z} + \chi_z q_z = 0 \end{cases}, \tag{17}$$

where $\beta_\alpha = \sqrt{\beta}B/2$. We introduce the coupling coefficients χ_α and χ_z [A.s.m^{-1}]. The potential difference between both electrodes of the patch V can be replaced by the electric charge variable. Also, by introducing the electrical angular frequency and the electrical damping ratio as

$$\omega_e = \frac{1}{\sqrt{LC}} \quad \text{and} \quad \zeta_e = \frac{R}{2}\sqrt{\frac{C}{L}}, \tag{18}$$

the previous electric equation in Eq. (17) can be rewritten as an electrical oscillator using the $V(\ddot{Q}, \dot{Q})$ relation in Eq. (16) and the electro-mechanical system becomes

$$\begin{cases} \ddot{q}_{\alpha z} + 2\zeta_\alpha^{tot}\omega_\alpha \dot{q}_{\alpha z} + \left(\omega_\alpha^2 + \dfrac{\beta_\alpha^2}{I^*C}\chi_\alpha^2\right) q_{\alpha z} + \bar{\theta}_\alpha \ddot{q}_z + \dfrac{\beta_\alpha^2}{I^*C}\chi_\alpha\chi_z q_z = M_v C_L(t) + \dfrac{\beta_\alpha^2}{I^*C}\chi_\alpha Q \\ \ddot{q}_z + 2\zeta_z^{tot}\omega_z \dot{q}_z + \left(\omega_z^2 + \dfrac{1}{M^*C}\chi_z^2\right) q_z + \bar{\theta}_z \ddot{q}_{\alpha z} + \dfrac{1}{M^*C}\chi_\alpha\chi_z q_{\alpha z} = F_v C_L(t) + \dfrac{1}{M^*C}\chi_z Q \\ \ddot{Q} + 2\zeta_e\omega_e \dot{Q} + \omega_e^2 Q = \omega_e^2(\chi_\alpha q_{\alpha z} + \chi_z q_z) \end{cases}. \tag{19}$$

One can define coupling factors of both structural oscillators with the piezoelectric shunt as

$$k_\alpha = \frac{1}{\omega_\alpha}\frac{\beta_\alpha}{\sqrt{I^*C}}\chi_\alpha \quad \text{and} \quad k_z = \frac{1}{\omega_\alpha}\frac{1}{\sqrt{M^*C}}\chi_z\,. \tag{20}$$

Note that the bending coupling factor k_z is not expressed as the standard defined one k_z^{std} [13, 14] and $k_z = \frac{\omega_z}{\omega_\alpha}k_z^{std}$. Therefore, system in Eq. (19) becomes

$$\begin{cases} \ddot{q}_{\alpha z} + 2\zeta_\alpha^{tot}\omega_\alpha \dot{q}_{\alpha z} + \hat{\omega}_\alpha^2 q_{\alpha z} + \bar{\theta}_\alpha \ddot{q}_z + \dfrac{\Omega_{\alpha z}^2}{I_r} q_z = M_v C_L(t) + \omega_\alpha k_\alpha \dfrac{\beta_\alpha}{\sqrt{I^*C}} Q \\ \ddot{q}_z + 2\zeta_z^{tot}\omega_z \dot{q}_z + \hat{\omega}_z^2 q_z + \bar{\theta}_z \ddot{q}_{\alpha z} + \Omega_{\alpha z}^2 I_r q_{\alpha z} = F_v C_L(t) + \omega_\alpha k_z \dfrac{1}{\sqrt{M^*C}} Q \\ \ddot{Q} + 2\zeta_e\omega_e \dot{Q} + \omega_e^2 Q = \omega_e^2(\chi_\alpha q_{\alpha z} + \chi_z q_z) \end{cases}. \tag{21}$$

We introduce the open-circuit natural angular frequencies $\hat{\omega}_\alpha$, $\hat{\omega}_z$ in torsion and bending, respectively, the square root of the reduced lineic inertia I_r and the angular frequency coupling term between the two structural oscillators $\Omega_{\alpha z}$, as

$$\hat{\omega}_\alpha^2 = \omega_\alpha^2(1 + k_\alpha^2), \quad \hat{\omega}_z^2 = \omega_z^2\left(1 + \frac{\omega_\alpha^2}{\omega_z^2}\,k_z^2\right), \quad \Omega_{\alpha z}^2 = \omega_\alpha^2\, k_\alpha\, k_z, \tag{22}$$

$$I_r = \frac{1}{\beta_\alpha}\sqrt{\frac{I^*}{M^*}} = \frac{1}{\beta_\alpha}\sqrt{\frac{I_{tot}}{M_{tot}}\frac{\int_0^s \Phi_\alpha^2(y)\,dy}{\int_0^s \Phi_z^2(y)\,dy}} = \frac{1}{\beta_\alpha}\sqrt{\frac{I_{tot}}{M_{tot}} S_{\Phi\alpha z}} \quad \text{with} \quad S_{\Phi\alpha z} \approx 2. \tag{23}$$

Therefore, we propose to change the variables for the electric charge and both oscillators generalized coordinates to

$$\bar{q}_{\alpha z} = \frac{q_{\alpha z}}{D}, \quad \bar{q}_z = \frac{q_z}{I_r D} \quad \text{and} \quad \bar{Q} = \frac{1}{\omega_\alpha}\frac{\beta_\alpha}{\sqrt{I^*C}}\frac{Q}{D}, \tag{24}$$

such as, the system in Eq. (21) becomes

$$\begin{cases} \ddot{\bar{q}}_{\alpha z} + 2\zeta_\alpha^{tot}\omega_\alpha \dot{\bar{q}}_{\alpha z} + \hat{\omega}_\alpha^2 \bar{q}_{\alpha z} + \bar{\theta}_{\alpha z}\ddot{\bar{q}}_z + \Omega_{\alpha z}^2 \bar{q}_z = \bar{M}_v C_L(t) + \omega_\alpha^2 k_\alpha \bar{Q} \\ \ddot{\bar{q}}_z + 2\zeta_z^{tot}\omega_z \dot{\bar{q}}_z + \hat{\omega}_z^2 \bar{q}_z + \bar{\theta}_{\alpha z}\ddot{\bar{q}}_{\alpha z} + \Omega_{\alpha z}^2 \bar{q}_{\alpha z} = \bar{F}_v \frac{1}{I_r} C_L(t) + \omega_\alpha^2 k_z \bar{Q} \\ \ddot{\bar{Q}} + 2\zeta_e\omega_e \dot{\bar{Q}} + \omega_e^2 \bar{Q} = \omega_e^2(k_\alpha \bar{q}_{\alpha z} + k_z \bar{q}_z) \end{cases}. \tag{25}$$

One can note that $\bar{\theta}_{\alpha z} = \bar{\theta}_\alpha I_r = \bar{\theta}_z \frac{1}{I_r}$. Adding the Van der Pol equation for the fluid forcing model, the dimensionless time $\tau = \omega_v t$ is once again introduced. The structure to fluid frequency ratios in short-circuit remain defined as $\delta_i = \frac{1}{St\,U_{r_i}}$ (with $i = \{\alpha, z\}$). Moreover, the electric to fluid frequency ratios

is defined as $\delta_e = \omega_e/\omega_v$. Then, the piezo-elasto-hydrodynamic dimensionless system can finally be written as

$$\begin{cases} \ddot{\bar{q}}_{\alpha z} + 2\zeta_\alpha^{tot}\delta_\alpha \dot{\bar{q}}_{\alpha z} + \hat{\delta}_\alpha^2 \bar{q}_{\alpha z} + \bar{\theta}_{\alpha z}\ddot{\bar{q}}_z + \Delta_{\alpha z}^2 \bar{q}_z = \bar{M}_v q_v + \delta_\alpha^2 k_\alpha \bar{Q} \\ \ddot{\bar{q}}_z + 2\zeta_z^{tot}\delta_z \dot{\bar{q}}_z + \hat{\delta}_z^2 \bar{q}_z + \bar{\theta}_{\alpha z}\ddot{\bar{q}}_{\alpha z} + \Delta_{\alpha z}^2 \bar{q}_{\alpha z} = \bar{F}_v \frac{1}{I_r} q_v + \delta_\alpha^2 k_z \bar{Q} \\ \ddot{\bar{Q}} + 2\zeta_e \delta_e \dot{\bar{Q}} + \delta_e^2 \bar{Q} = \delta_e^2 (k_\alpha \bar{q}_{\alpha z} + k_z \bar{q}_z) \\ \ddot{q}_v + \varepsilon\left(q_v^2 - 1\right)\dot{q}_v + q_v = A_z \ddot{\bar{q}}_z + A_\alpha \ddot{\bar{q}}_{\alpha z} \end{cases}, \tag{26}$$

with $\Delta_{\alpha z}^2 = \delta_\alpha^2 k_\alpha k_z$ the dimensionless structural coupling factor. One can also note that the total amplitude derived from the contribution of both modes is defined as $\tilde{w}_z = \bar{q}_{\alpha z} + I_r \bar{q}_z$ since we keep a total dimensionless amplitude reduced by the characteristic length D only.

4.2. Confrontation to experimental data

Optimal values of the electrical angular frequency ω_e and damping ratio ζ_e which maximize reduction of amplitude of vibration are known for linear system excited by external forcing (see [13] for example). When targeting the torsion mode, the optimal electrical parameters can be defined as

$$\omega_e^{optim} \approx \hat{\omega}_\alpha = \omega_\alpha \sqrt{1 + k_\alpha^2}, \quad \zeta_e^{optim} \approx \sqrt{\frac{3}{8}} k_\alpha \quad \text{with} \quad k_\alpha = \sqrt{\frac{\hat{\omega}_\alpha^2 - \omega_\alpha^2}{\omega_\alpha^2}}. \tag{27}$$

To the best knowledge of the authors, no optimal electrical parameters are available in the literature for piezo-elasto-hydrodynamic coupled system under lock-in condition. As initial values, we use the previous optimal parameters since their are valid for weakly coupled VIV where external excitation can be seen as a sinus forcing. In this case, the previous electrical angular frequency and damping ratio set are optimal for amplitude reduction of the torsion mode. In order target the bending mode damping as well, the electrical frequency would have to be moved in direction of the bending mode frequency. From experimental results in [7], coupling coefficients are evaluated to $k_\alpha = 8.5\,\%$ and $k_z = \frac{\omega_z}{\omega_\alpha} k_z^{std} = 5.1\,\%$ with $k_z^{std} = 4.7\,\%$ (in reference to classical definition of the coupling factor [13, 14] and the way we define it in Eq. (20)). Then, based on the coupling coefficients, best fitted electrical parameters are set to $\omega_e = 1.03\,\omega_e^{optim}$ and $\zeta_e = 1.4\,\zeta_e^{optim}$ as can be seen in Fig. 7 and 8.

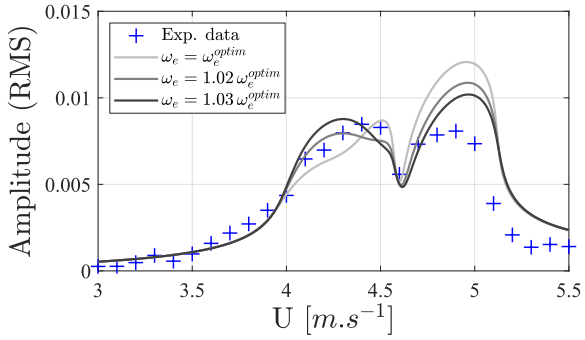

Figure 7: Coupled model with shunt versus experiment; Using the fitted parameters summarized in Tab. 1, $\zeta_e = \zeta_e^{optim}$ and three sets of parameter ω_e.

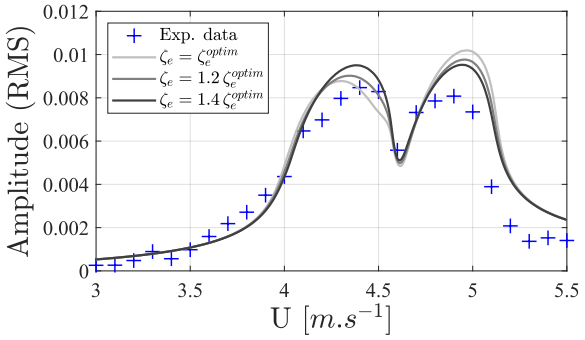

Figure 8: Coupled model with shunt versus experiment; Using the fitted parameters summarized in Tab. 1, $\omega_e = 1.03\,\omega_e^{optim}$ and three sets of parameter ζ_e.

Final results obtained by numerical integration, with and without the piezoelectric shunt, are confronted to experimental results in Fig. 9. One can observe that the vibration mitigation at lock-in obtained with the piezo-elasto-hydrodynamic model in Eq. (26) is close to those obtained experimentally in [7]. The maximal relative error measured in lock-in regions is only about 12 %. Still, we can also observe an increase of RMS amplitudes from the piezo-elasto-hydrodynamic

model, for $U \geqslant 5.1\, m.s^{-1}$, in comparison to the VIV model. A first assumption would be that the VIV coupled system model has to be improved. The coupling model between the electrical oscillator and the structural oscillator of the bending mode could also be subject to improvement.

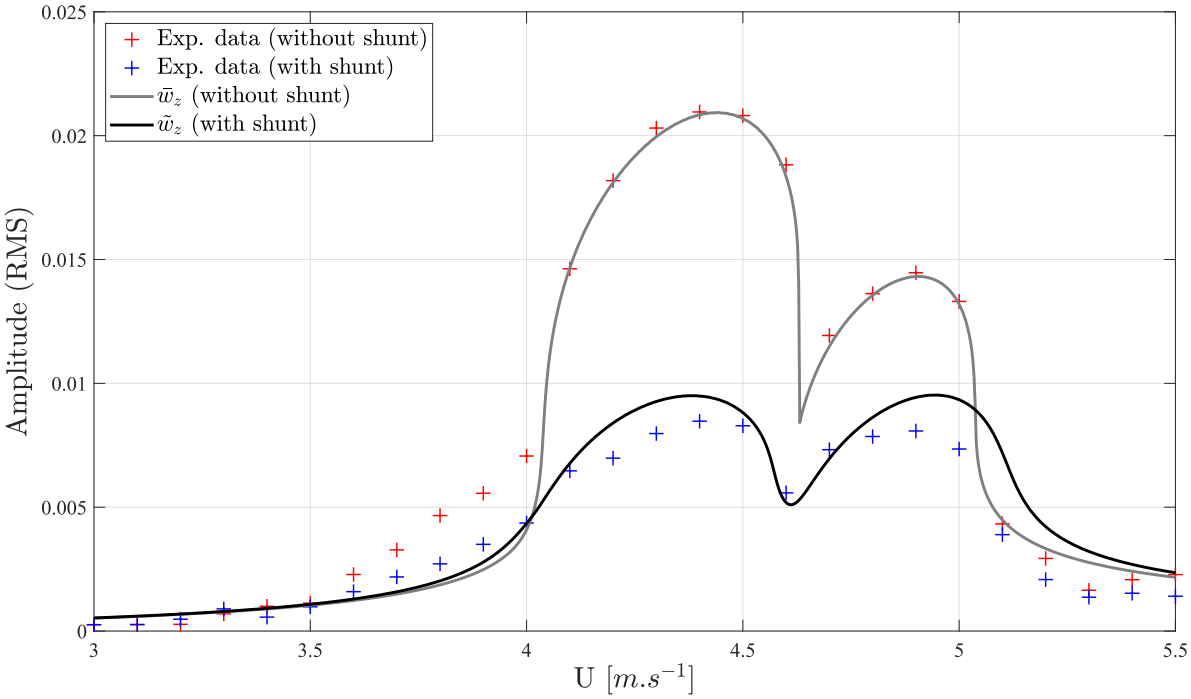

Figure 9: Dimensionless total RMS amplitude of vibration with and without resonant piezoelectric shunt : coupled model versus experiment; Numerical results obtained with best fitted parameters summarized in Tab. 1.

5. CONCLUSIONS

A fluid-structure-piezoelectric low order model of a truncated NACA-profile hydrofoil has been proposed in order to analyze vibration mitigation of vortex-induced vibrations. The first torsion mode and the second bending mode of the structure have been scrutinized in a short range of Reynolds number $2.55 \times 10^5 \leq Re \leq 4.68 \times 10^5$. Based on the work of Amandolese et al. [6], hydroelastic VIV model has been expressed with a set of 6 unknown parameters. Using a single Kármán vortex shedding excitation, parameters have been identified by confrontation with experimental data to best fit the amplitude and frequency response at both lock-in. Piezo-elasto-hydrodynamic model with fitted electrical parameters shows vibration reduction with an accuracy of 12 % in comparison to experimental data. Obtained results with the two models (with and without piezoelectric shunt) are promising and the control strategy is compliant with experimental data. Still, we believe they can be improved, especially for the piezo-elasto-hydrodynamic model. Future work includes improvement of the piezo-elasto-hydrodynamic model as well as an analytic optimization of R and L parameters for strong VIV coupling (i.e. frequency lock-in). Perspectives also includes the addition of a second Van der Pol oscillator in order to consider a second fluid excitation mechanism.

ACKNOWLEDGEMENTS

The authors would like to express sincere gratitude to the members of the *Institut de Recherche de l'Ecole Navale* (IRENav), more particularly to Yann Watine and Céline Gabillet, for their assistance and data sharing. The authors also acknowledge the Agence de l'Innovation de Défense (AID) and the Agence Nationale de la Recherche (ANR) for the support of the project HYDRAVIB (ANR-22-ASTR-0012).

REFERENCES

1. W. K. Blake. Excitation of Plates and Hydrofoils by Trailing Edge Flows. *Journal of Vibration, Acoustics, Stress, and Reliability in Design*, 106(3):351–363, 07 1984.
2. G.H. Toebes and P.S. Eagleson. Hydroelastic vibrations of flat plates related to trailing edge geometry. *Journal of Basic Engineering*, 83(4):671–678, 12 1961.
3. P. Francois, J.-A. Astolfi, and X. Amandolese. Experimental analysis of hydrofoil hydroelastic trailing edge vibrations. *Journal of Fluids and Structures*, 2023.
4. M.P. Paidoussis, S.J. Price, and E. de Langre. *Fluid-Structure Interactions: Cross-Flow-Induced Instabilities*. Cambridge University Press, 2010.
5. M.L. Facchinetti, E. De Langre, and F. Biolley. Coupling of structure and wake oscillators in vortex-induced vibrations. *Journal of Fluids and Structures*, 19(2):123–140, 2004.
6. X. Amandolese, C. Gabillet, and Y. Watine. Adaptation of the facchinetti, de langre and biolley model for the hydroelastic vortex-induced vibrations of a cantilevered flat plate. *Journal of Fluids and Structures*, 124:104017, 2024.
7. Y. Watine, B. Lossouarn, C. Gabillet, J.-F. Deü, and J.-A. Astolfi. Effect of a resonant piezoelectric shunt on the structural vibrations of a truncated hydrofoil. In *10th ECCOMAS Thematic Conference on Smart Structures and Materials*, pages 226–237. Dept. of Mechanical Engineering & Aeronautics University of Patras, 2023.
8. M. Geradin and J.R. Daniel. *Mechanical Vibrations - Theory and application to structural dynamics*. John Wiley & Sons, 2015.
9. T. Theodorsen. General theory of aerodynamic instability and the mechanism of flutter. Technical report, Aerodynamic Flutter, American Institute of Aeronautics and Astronautics, 1935.
10. R.D. Blevins. *Flow-induced vibration*. Van Nostrand Reinhold, New York, second edition, 1990.
11. T. Sarpkaya. Fluid forces on oscillating cylinders. *Journal of the Waterway, Port, Coastal and Ocean Division*, 104(3):275–290, 1978.
12. T. Sarpkaya. Vortex-induced oscillations: A selective review. *Journal of Applied Mechanics*, 46(2):241–258, 1979.
13. O. Thomas, J. Ducarne, and J.-F. Deü. Performance of piezoelectric shunts for vibration reduction. *Smart Materials and Structures*, 21(1):015008, 2012.
14. J. Ducarne, O. Thomas, and J.-F. Deü. Placement and dimension optimization of shunted piezoelectric patches for vibration reduction. *Journal of Sound and Vibration*, 331(14):3286–3303, 2012.
15. N.W. Hagood and A. von Flotow. Damping of structural vibrations with piezoelectric materials and passive electrical networks. *Journal of Sound and Vibration*, 146(2):243–268, 1991.
16. L. Pernod, B. Lossouarn, J.-A. Astolfi, and J.-F. Deü. Vibration damping of marine lifting surfaces with resonant piezoelectric shunts. *Journal of Sound and Vibration*, 496:115921, 2021.
17. B. Lossouarn, M. Aucejo, J.-F. Deü, and B. Multon. Design of inductors with high inductance values for resonant piezoelectric damping. *Sensors and Actuators A: Physical*, 259:68–76, 2017.
18. O. Thomas, J.F. Deü, and J. Ducarne. Vibrations of an elastic structure with shunted piezoelectric patches: efficient finite element formulation and electromechanical coupling coefficients. *International Journal for Numerical Methods in Engineering*, 80(2):235–268, 2009.